Composites Part B 201 (2020) 108337

Contents lists available at ScienceDirect

Composites Part B

journal homepage: www.elsevier.com/locate/compositesb

Elastomeric high-κ composites of low dielectric loss tangent: Experiment and simulation

Youngpyo Ko [a,b,1], Hyungsuk Yoon [c,d,1], Seulki Kwon [e,1], Hyunjung Lee [f], Min Park [b], Insu Jeon [d], Jung Ah Lim [g], Seungjun Chung [b], Sang-Soo Lee [a,b,*], Bong June Sung [e,**], Jong-Ho Kim [c,***], Heesuk Kim [b,h,****]

[a] KU-KIST Graduate School of Converging Science and Technology, Korea University, Seoul, 02841, Republic of Korea
[b] Photo-electronic Hybrids Research Center, Korea Institute of Science and Technology (KIST), Seoul, 02792, Republic of Korea
[c] Center for Mechanical Metrology, Korea Research Institute of Standards and Science (KRISS), Daejeon, 34113, Republic of Korea
[d] School of Mechanical Systems Engineering, Chonnam National University, Gwangju, 61186, Republic of Korea
[e] Department of Chemistry, Sogang University, Seoul, 04107, Republic of Korea
[f] School of Advanced Materials Engineering, Kookmin University, Seoul, 02707, Republic of Korea
[g] Center for Opto-Electronic Materials and Devices, Korea Institute of Science and Technology (KIST), Seoul, 02792, Republic of Korea
[h] Nano-Materials and Engineering, Korea University of Science and Technology (UST), Daejeon, 34113, Republic of Korea

ARTICLE INFO

Keywords:
Nanocomposites
Dielectric properties
Capacitive-pressure sensing
Simulation

ABSTRACT

As practical interest in wearable electronic devices and biomimetic transducers increases, the demand for elastomers with excellent dielectric behavior as well as good mechanical properties is growing. Herein, we propose a new concept of carbon black (CB)-embedded polydimethylsiloxane (PDMS) composites with high dielectric properties *via* a one-pot process. The dispersant-grafted $CB_{3wt\%}$/PDMS composites show an enhanced dielectric constant of 1090 with low loss tangent as low as 0.45 at 100 Hz, which is 340- and 145-fold higher than those of the pure PDMS and dispersant-free $CB_{3wt\%}$/PDMS, respectively. Experimental and simulation studies demonstrate that the dielectric properties of CB/PDMS composites depend on the CB dispersion in the PDMS matrix, which is influenced by the chain length of dispersant and the amount of residual dispersant. As a proof of concept, the capacitive pressure sensor based on CB/PDMS flat structure has been demonstrated, exhibiting 46-fold larger capacitance change than the pure PDMS based sensor. These results indicate that the sensor sensitivity can be significantly improved without additional micro-structuring and the large capacitance change enhances a tolerance to external noise sources. We believe that the elastomers with high dielectric properties show great potential for electronic applications including capacitive pressure sensors that should respond to various input pressures.

1. Introduction

Dielectric elastomers have received renewed attention for realizing biomimetic transducers such as skin sensors and artificial muscles [1–4]. Their low dielectric permittivity limits, however, the use of dielectric elastomers in these applications. Nano-composites with high-dielectric fillers dispersed in elastomeric matrix have been investigated to enhance their dielectric properties [5–9]. Along with high dielectric properties, the excellent mechanical behavior including stretchability and dimensional stability is essential, thus requiring the small volume fraction of fillers in elastomeric matrix. In the case of ceramic or metal fillers, nano-composites need the large volume fraction of these fillers for high dielectric properties [10–12]. In contrast, nanoscale carbonaceous materials such as carbon nanotube (CNT) have shown promise in

* Corresponding author. KU-KIST Graduate School of Converging Science and Technology, Korea University, Seoul, 02841, Republic of Korea.
** Corresponding author. Department of Chemistry, Sogang University, Seoul, 04107, Republic of Korea.
*** Corresponding author. Center for Mechanical Metrology, Korea Research Institute of Standards and Science (KRISS), Daejeon, 34113, Republic of Korea.
**** Corresponding author. Photo-electronic Hybrids Research Center, Korea Institute of Science and Technology (KIST), Seoul, 02792, Republic of Korea.
E-mail addresses: s-slee@kist.re.kr (S.-S. Lee), bjsung@sogang.ac.kr (B.J. Sung), jhk@kriss.re.kr (J.-H. Kim), heesukkim@kist.re.kr (H. Kim).
[1] Authors contributed equally to this work.

https://doi.org/10.1016/j.compositesb.2020.108337
Received 25 May 2020; Received in revised form 21 July 2020; Accepted 4 August 2020
Available online 18 August 2020
1359-8368/

dielectric nano-composites [13]. With a large aspect ratio, the special kind of aligned CNT filler can act as a microcapacitor, which results in a high dielectric constant of the composites. However, the large aspect ratio makes the CNTs strongly agglomerated in the elastomer, thus requiring intensive chemical/or physical modifications of CNT surfaces or special blending techniques for dispersion [13–15].

As an alternative, conductive carbon black (CB) has great potential for use in dielectric fillers because of its reliable electrical properties and relatively easy dispersion compared to the CNTs. A few studies of CB-elastomer composites with enhanced dielectric properties have been reported [16–18]. For CB-elastomer composites with low dielectric loss tangent, the dielectric constants are only several times higher than those of the pure elastomers [17,18]. Whereas, in the case of CB-elastomer composite with high dielectric constant, the CB filler also significantly increases the dielectric loss tangent to around 5, which might be owing to poor dispersion of dispersant-free CBs in the natural rubber [16]. Therefore, an alternative method of uniformly dispersing CBs in the elastomer to achieve the reliable dielectric properties and low dielectric loss tangents is highly desirable.

Here, we demonstrate a new concept of CB-embedded polydimethylsiloxane (PDMS) composites exhibiting an enhanced dielectric constant of 1090 with low loss tangent as low as 0.45 at 100 Hz. These dielectric properties are attributed to the fact that the CBs without loss of their intrinsic electrical properties are well-dispersed in PDMS. It was simply achieved by functionalizing the CBs with alkyltrimethoxysilanes and blending with PDMS, simultaneously, while most previous methods modified the carbon materials for their dispersion followed by compounding with the matrix [14,19,20]. Experimental and simulation studies show that the dielectric properties of CB-embedded composites are highly dependent on the chain length of alkyltrimethoxysilanes, thus understanding the relationship between the chain length of surfactant and the CB dispersion in the elastomer being critical. As a proof of concept, we show capacitive pressure sensors based on CB-embedded PDMS composites. Most previous capacitive pressure sensors are based on delicate microstructures such as pyramid-shaped pure PDMS films for their high sensitivity [21,22]. However, these sensors suffer from interference from external noise sources owing to the small capacitance change [21–24], and present relatively slow dynamic response and low reliability at heavy input loadings, thereby leading to limited applications. In contrast, the pressure sensors based on CB-embedded composites with high dielectric constant show large capacitance changes despite small displacements, thus enhancing a tolerance to external noise sources. In addition, these sensors exhibit an excellent reliability.

2. Experimental section

2.1. Fabrication of CB-embedded PDMS dielectric composite

Conductive CBs (Cabot Co., Black Pearls 2000, 1635 m^2/g surface area) with various amounts of alkyltrimethoxysilanes were dispersed in PDMS/chloroform mixtures, followed by solvent-evaporation at 90 °C for 72 h. The alkyltrimethoxysilanes (ATMSs) with three different alkyl-chain lengths, i.e., octyltrimethoxysilane (OTMS), dodecyltrimethoxysilane (DDTMS), and octadecyltrimethoxysilane (ODTMS), were used. OTMS and ODTMS were purchased from Sigma-Aldrich, and DDTMS was obtained from Alfa-Aesar. After solvent-evaporation, a curing agent was added to the CB/PDMS mixture. The final paste was mixed for 7 min and cured at 130 °C for 90 min.

2.2. Characterization

The functional groups of the CB samples were characterized using a Nicolet iS 10 fourier-transform infrared spectroscopy (FT-IR) spectrometer (Thermo Fisher Scientific, Inc.). The dispersibility of CBs in chloroform/PDMS mixtures was examined by using optical microscopy (OM, DM 2500 M, Leica) and transmission electron microscope (TEM, Tecnai G2, FEI). Thermogravimetric analysis (TGA) was used to determine the ATMS content at the CB sufaces under an N_2 using a Q50 analyzer (TA instruments). The dielectric properties of the composites were characterized by an impedance analyzer (E4980A, KEYSIGHT) after sputtering of a platinum electrode on top of the film. Five or more specimens of each sample were tested to obtain the average dielectric properties.

2.3. Simulation method

We employ a coarse grained model to mimic ATMS-CB/PDMS composites and investigate the effects of ATMS and its chain length on the dispersion of CB fillers. A CB particle is modeled as a large spherical nanoparticle comprised of 500 small spheres (white spheres in Fig. 4(a)) of diameter σ and mass m, which are the units of length and mass in our simulations, respectively. Nonbonding interactions between two spheres are described by a truncated and shifted Lennard-Jones potential, $U_{LJ}(r)$ as follows:

$$U_{LJ}(r) = 4\varepsilon\left[\left(\frac{\sigma}{r}\right)^{12} - \left(\frac{\sigma}{r}\right)^{6}\right] - \varepsilon_{rc}, r < r_c,$$

where r is the distance between two spheres. We set $\varepsilon = 2k_BT$ and $r_c = 2.5\sigma$ such that 500 spheres aggregate strongly with one another and form a stable large CB nanoparticle of diameter $d_{np} \approx 8.5\sigma$. $k_B$and T denote the Boltzmann constant and temperature, respectively, thus k_BT is the energy unit in our simulations. We employ a harmonic bonding potential, i.e. $U_b(r) = K(r - r_0)^2$where $K = 1000k_BT/\sigma^2$ and $r_0 = \sigma$, between two adjacent spheres within a distance 1.05σ to tightly bind spheres and maintain its shape (Fig. 4(a)). ATMS is modeled as a short chain molecule comprised of n_{chain} monomers of diameter σ and mass m (yellow particles in Fig. 4(b)). Two neighbor monomers are also bonded with the harmonic potential, $U_b(r)$.

ATMS molecules are either attached on the surface of CB with a surface number density ρ_{graft} or dissolved in bulk solutions with a molecule number density $\rho_{residual}$ (Fig. 4(g)). We graft the ATMS molecules to the small spheres at the surface of the CB particle by connecting the end monomer of the ATMS molecule with the surface monomer *via* $U_b(r)$. ρ_{graft} is, then, defined by the fraction of the small spheres at the CB surface that are chemically bonded with ATMS molecules. $\rho_{residual}$ is defined as the number density of residual ATMS molecules that are not bonded with CB. We employ periodic boundary conditions along xyz directions with a cubic simulation cell of dimension $L = 4$. Nonbonding interactions either between chain monomers or between chain monomers and CB spheres are described by a purely repulsive Lennard-Jones potential ($U_{LJ}(r)$) with a cut-off distance $r_c = 1.122$ and. $\varepsilon = k_BT$.

We perform steered molecular dynamics (SMD) simulations to investigate the effect of ATMS on the dispersion of CB particles by calculating a free energy $F(h)$ as a function of the gap (h) between two CBs. We evolve the system by solving Langevin equation *via* the LAMMPS simulator [25] as follows:

$$m\frac{d^2\boldsymbol{r}}{dt} = -\nabla_r U - \xi\frac{d\boldsymbol{r}}{dt} + \delta F_r(t),$$

where U is the inter-particle interaction including U_b and U_{LJ}, and ξ is a friction coefficient. r is the position vector of particles and $\delta F_r(t)$ denotes a random force that satisfies the fluctuation-dissipation theorem, i.e. $\delta F_r(t)\delta F_r(t') = 2\xi k_BT\delta(t - t')$. We use the velocity-Verlet integrator and the integration time step is 0.005τ, where τ is the reduced time unit, i.e. $\tau \equiv \sqrt{\frac{m\sigma^2}{k_BT}}$. In SMD simulations, there are two CBs separated by$R = 20$, where R is the center-to-center distance. A guiding potential, i.e. $h(R) = \frac{1}{2}k(R - \lambda)^2$, is added to one CB particle while the other is fixed at its initial position. We follow a constant-velocity SMD scheme [26], where λ changes linearly with a velocity $v = -5{*}10^{-4}$ and a force constant = $10^4\ k_BT/\sigma^2$. According to Jarzynski's equality [27], a free energy

difference $\Delta F(R)$ between two states $R = \lambda_0$ and $R = \lambda_t$ relates to the amount of work (W) by $\Delta F = F(\lambda_t) - F(\lambda_0) = \beta^{-1}\log\exp(-\beta W_{0\to t})$.We equilibrate the initial configuration with fixing $\lambda = 20$, and then start SMD simulations to calculate work by changing λ from $\lambda_0 = 20$to $\lambda_t = 8$. We change n_{chain} and ρ_{graft} in order to investigate effects of a chain length and a surface density and calculate a free energy profile $\Delta F(R)$ for a given n_{chain}, ρ_{graft} and $\rho_{residual}$. We average the number of work over 100 different SMD trajectories for each set of parameters (n_{chain}, ρ_{graft}, $\rho_{residual}$).

2.4. Sensor fabrication and evaluation

The CB/PDMS-I and CB/PDMS-II composites were fabricated by adding 0.707 and 0.943 mmol ODTMSs into the PDMS mixture with 2 wt % p-CBs, respectively. The dielectric layer with 280 μm in thickness was coated on the Cu plate, followed by curing 130 °C for 90 min. And then the upper electrode was formed on the dielectric layer by using a silicon-based conductive adhesive with 6 mm in diameter and 100 μm in thickness. The Pt wire as a signal line was connected to the two electrodes. In the capacitance measurement versus input pressure, the pressure was controlled by using weights that consists of 7 pieces of 50 g, 5 pieces of 100 g and tare weight of 50 g. In order to minimize the environmental noise, the loading tester was fabricated using polyoxymethylene with excellent mechanical strength and low electrical conductivity. The probe tip has 6 mm in diameter. The capacitance was measured usign a precision impedance analyzer (Agilient 4294A).

3. Results and discussion

3.1. Facile fabrication of CB-embedded PDMS composites

The CB-embedded composites with high dielectric properties were simply prepared by functionalizing the CBs without loss of their pristine electrical conductivity and by dispersing the CBs into the PDMS matrix, simultaneously. As shown in Fig. 1(a), the agglomerated CBs were mixed with alkyltrimethoxysilanes and PDMS base in chloroform, followed by solvent-evaporation at 90 °C for 72 h. After adding a curing agent into this mixture, the dielectric composites were fabricated. Considering the dispersion of CB particles and solubility parameter of PDMS base, chloroform was selected as a solvent (Fig. S1) [28]. The alkyltrimethoxysilanes (ATMSs) with three different alkyl-chain lengths, i.e., octyltrimethoxysilane (OTMS), dodecyltrimethoxysilane (DDTMS), and octadecyltrimethoxysilane (ODTMS), were used (Fig. 1(b)). It is because carbon materials functionalized with alkyl chains containing 12 or more CH_2 groups are known to have excellent dispersibility in hydrophobic media [29,30]. During solvent-evaporation, the hydroxyl groups of the CB surfaces chemically react with ATMSs. The pristine CB (p-CB) particles have many oxygen-containing functional groups such as hydroxyl groups on their surfaces, thus leading to covalent-linkages with ATMSs without pre-treatment like oxidation (Fig. S2). The FT-IR spectrum of the ODTMS-modified CB sample reveals two characteristic peaks at 2850 and 2920 cm^{-1} due to C–H stretching in the long octadecyl chains [31], confirming the attachment of ODTMS molecules on the CB surface (Fig. S3). TGA supports the chemical grafting of ODTMS on the CB surface. Although pure ODTMS evaporates at 150–250 °C owing to the boiling temperature of 170 °C, the ODTMS-CB shows no weight loss at 150–250 °C and a 30 wt% loss at 350–550 °C, further demonstrating the successful chemical grafting of ODTMS molecules to the CB surface during solvent-evaporation.

As a proof of concept, the capacitive pressure sensor based on ODTMS-CB/PDMS composites has been demonstrated. Capacitive pressure sensor detects the change in capacitance induced by the change in the distance between two electrodes [32]. Capacitance is given by $C = \varepsilon A/d$, where ε, A, and d are the relative permittivity (dielectric

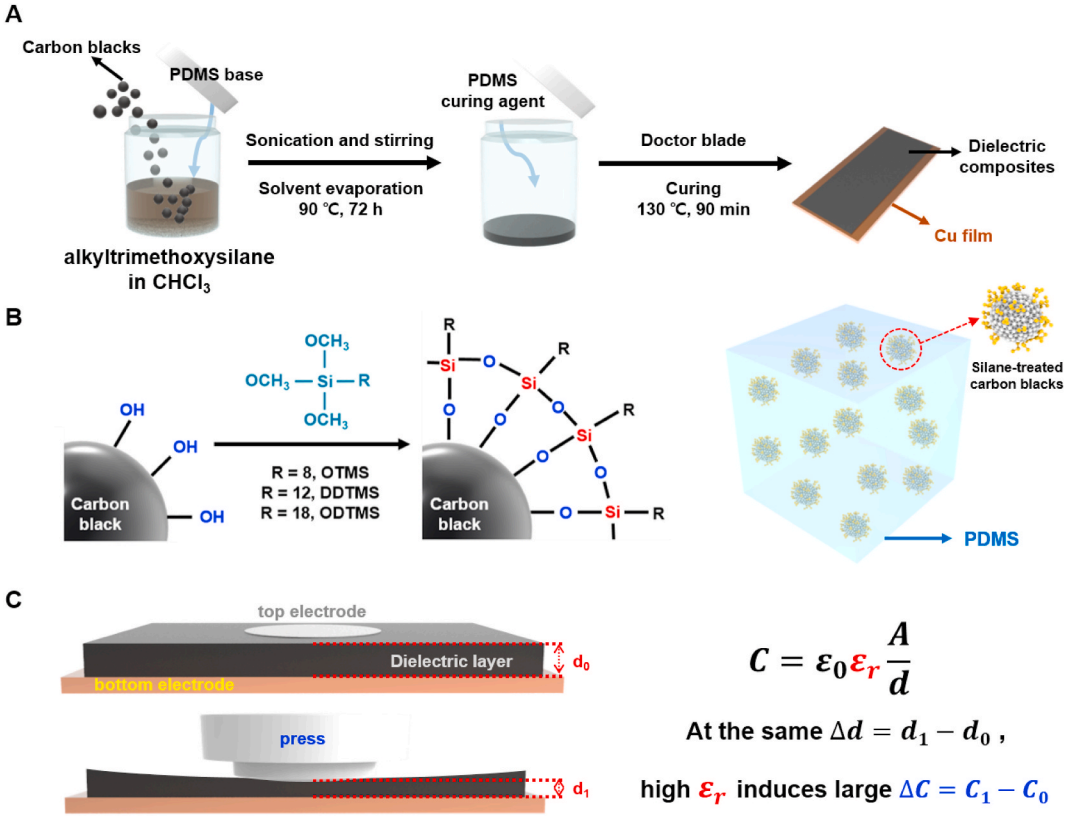

Fig. 1. Fabrication of CB-embedded PDMS dielectric composites. (a, b) Schematic illustration showing the preparation of PDMS composite with CBs chemically linked to ATMSs. (c) Capacitive pressure sensing based on CB/PDMS dielectric composites.

constant) of the dielectric materials, the area of the electrode, and the distance between two electrodes, respectively. Most capacitive pressure sensors have adopted delicate micro-structuring of pure dielectric elastomers, thus inducing the large capacitance change by increasing the changes in the distance between two electrodes and in the area of the electrode at light input loadings [33–35]. In contrast, the capacitive pressure sensor based on ODTMS-CB/PDMS composites in this study induces the large capacitance change despite small distance change, which is due to the high dielectric constant of the composites (Fig. 1(c)). The detailed explanations for the composite-based force sensor are discussed at a later point in this manuscript.

3.2. Dielectric properties of CB-embedded PDMS composites

The dielectric properties of PDMS composites with p-CB were chacterized as a function of the p-CB content (Fig. 2(a)-(b)). As the p-CB content increases to 3 wt% in PDMS, the dielectric constant and loss tangent increase to 7.5 and 0.029 at 100 Hz, respectively. The composites with CB contents higher than 3 wt% could not be fabricated owing to a failure in curing. Despite the addition of 3 wt% CBs into PDMS, the dielectric constant is only 2-fold higher than that of the pure PDMS, due to the agglomerated *p*-CBs in PDMS as shown in OM and TEM images of Figs. 3(a) and S4(a). The agglomerated conducting fillers minimize the number of microcapacitors, thus leading to a low dielectric constant [11,13]. When the ATMSs are added into the PDMS mixtures with 2 wt% p-CBs, the composites show a drastic increase in the dielectric constant (Fig. 2(c)–(d)). While OTMS has no effect on the dielectric constant of CB/PDMS composites, DDTMS and ODTMS molecules induce a significant increase in the dielectric constant. As DDTMS content increases to 1.4 mmol, the dielectric constant and loss tangent increase to 220 and 0.19 at 100 Hz, respectively. In case of ODTMS, its optimum content is 0.94 mmol, resulting in the dielectric constant of 317 and loss tangent of 0.28 at 100 Hz. This dielectric constant is 52-fold higher than that of the p-$CB_{2wt\%}$/PDMS composites without ODTMS. These results can be explained by the CB dispersion enhanced by ODTMS molecules. As shown in Fig. 3(b)-(d), S4(b)-(d) and S5, as the alkyl chain of the dispersants gets longer, the CB particles are dispersed better in PDMS. As a result, the ODTMS-functionalized CB particles exhibit the best dispersion. Due to their large surface area, well-dispersed CBs in the polymer matrix can act as microcapcitors, imparting high dielectric constants to the composites, as previously reported literatures [9,11,13]. For each microcapacitor in nanocomposites, two polarization mechanisms, i.e. interfacial polarization and dipolar polarization, are responsible for the high dielectric constant. Particularly, the interfacial polarization induced by the movement of charge carriers under an applied electric field mainly contributes in the CB/PDMS composites [13]. Furthermore, when 1.24 mmol ODTMSs were added into the PDMS mixture with 3 wt% p-CBs, the dielectric constant and loss tangent increase to 1090 and 0.45 at 100 Hz, respectively (Fig. 2(e)–(f)). It is 145-fold higher than that of the p-$CB_{3wt\%}$/PDMS composites without ODTMS, which currently represents one of the highest dielectric constants with low loss tangent reported for dielectric elastomers (Table S1) [13,17,18,36–38]. Fig. S6 exhibits the dielectric properties of ODTMS-modified CB/PDMS composites as a function of the frequency, indicating that the dielectric properties have a strong dependence on the frequency as reported in previous literatures [17]. At low frequencies, there is enough time to accumulate charges at the interface between the CB particles and the PDMS matrix, thus increasing the dielectric constants. In contrast, at high frequencies, the interfacial polarization cannot keep up with the frequency change, resulting in a decrease in the dielectric constant.

However, the CB/PDMS composites with ODTMS content higher than optimum show a decrease in the dielectric constant (Fig. 2(c)), owing to the re-agglomeration of CBs in PDMS (Fig. 3(e)–(f)). As shown in TGA data of Fig. S7, as the ODTMS content increases to 0.94 mmol (optimum point), the amount of ODTMS chemically linked to CB surfaces increases. However, when the ODTMS content higher than optimum is added into p-$CB_{2wt\%}$/PDMS, the amount of ODTMS reacted with CB is constant, indicating the formation of residual ODTMS molecules in CB/PDMS mixture. The re-agglomeration of CB particles with excess ODTMSs could be attributed to residual ODTMS molecules which do not participate in the chemical reaction with CBs. We tried to theoretically identify the effect of alkyl-chain length and residual ATMSs on the dispersion of CB particles in the PDMS matrix using SMD simulation.

3.3. Simulation study on the dispersion of CBs in PDMS

We performed SMD simulations to investigate the effect of ATMS and its chain length on the dispersion of CB fillers (Fig. 4(a)). We calculated a free energy $F(h)$ as a function of a gap distance, $h \equiv R - d_{np}$, between two CB particles (Fig. 4(b)). Here, R and d_{np} denote the distance between the centers of the mass of two CB particles and the diameter of the CB particle, respectively. Fig. 4(c) shows a free energy profile ($F(h)$) in the absence of ATMS. Since $F(h)$ has a very deep attractive well ($\sim 60\ k_BT$) at

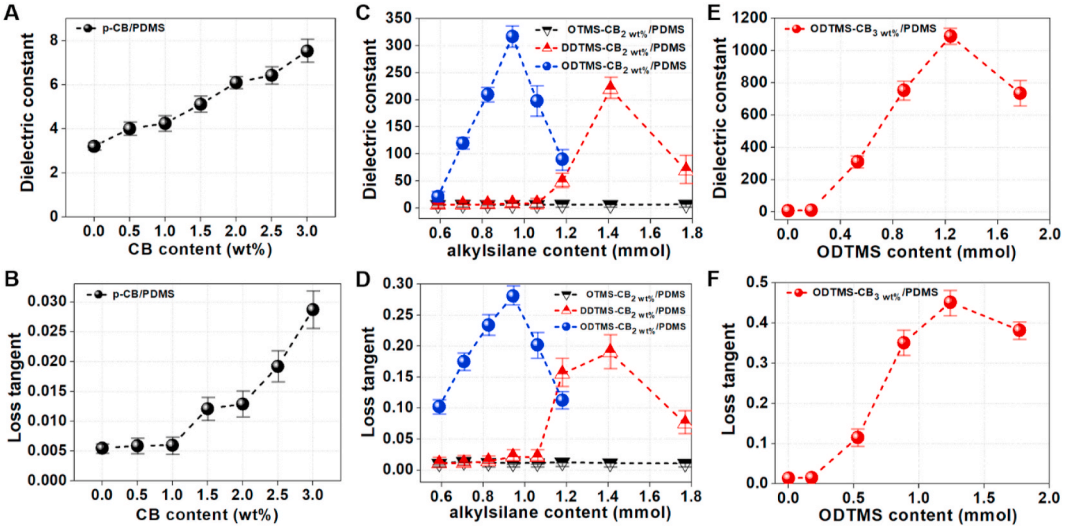

Fig. 2. Dielectric properties of CB-embedded PDMS dielectric composites. (a) Dielectric constant and (b) dielectric loss tangent of p-CB/PDMS composites as a function of the p-CB content. (c) Dielectric constant and (d) dielectric loss tangent of p-$CB_{2wt\%}$/PDMS composites with ATMS as a function of the ATMS content. (e) Dielectric constant and (f) dielectric loss tangent of p-$CB_{3wt\%}$/PDMS composites with ODTMS as a function of the ODTMS content.

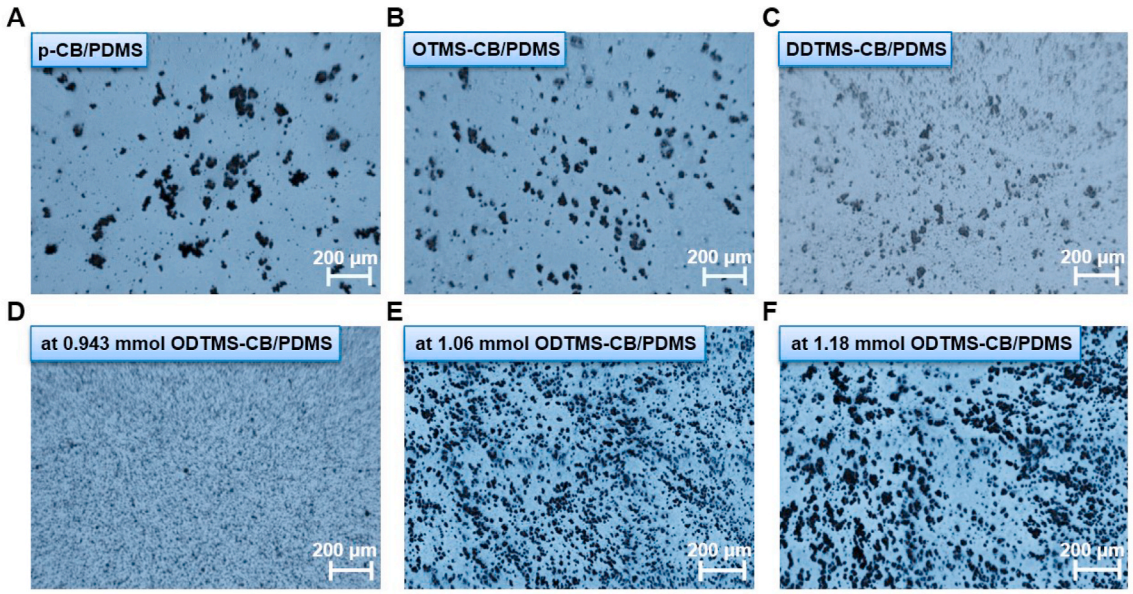

Fig. 3. Dispersibility of CBs in the dielectric composites. OM images of (a) p-CB, (b) OTMS-CB, (c) DDTMS-CB, and (d–f) ODTMS-CB in the PDMS/chloroform mixtures. The optimum contents of ATMSs were added into the PDMS/chloroform mixtures in ((b)–(d)). The excess ODTMSs were added into the PDMS/chloroform mixtures in ((e) and (f)).

small h, the CB particles would agglomerate, which is consistent with experimental results that the p-CB fillers are not dispersed well in PDMS mixture. When the ATMS molecules are grafted onto the CB surface, a repulsive free energy barrier around $h \approx 1$appears, as shown in the inset in Fig. 4(c). The repulsive barrier in $F(h)$ originates from an entropic contribution: the grafted chains confined between two CB particles may have a smaller number of possible conformations and lose the conformational entropy as two CB particles approach each other. In this study, we denote ΔF_1 and ΔF_2 as the attractive well depth and the repulsive barrier height, respectively, which relate closely to the dispersibility of CB fillers: the dispersibility would be increased as either ΔF_1 or ΔF_2 increases (note that ΔF_1 has a negative value).

In experiments, the ATMSs are either grafted to CB fillers or remain in the PDMS matrix. The ratio between grafted and residual ATMSs varies depending on the total amount of ATMSs added. It is hard in experiments to measure the ratio accurately. In order to investigate the effect of both grafted and residual ATMSs on CB dispersion, we change ρ_{graft} and $\rho_{residual}$. After a certain amount of ATMSs added, chemical grafting would be saturated and then the introduction of additional ATMSs will increase only the concentration of residual ATMSs. Fig. 4(d) shows the effects of grafted molecules on $F(h)$ where there is no excess molecules in mixture ($\rho_{residual} = 0$) for different chain length. A black line indicates $F(h)$ between two pristine CB particles for comparison (same in Fig. 4(c)). As shown in Fig. 4(d), the magnitude of the attractive well depth becomes smaller and the repulsive barrier becomes higher as ρ_{graft} increases. An increase of both ΔF_1 and ΔF_2 is more prominent in the longer chain (see lower panel in Fig. 4(d)) such that ΔF_1 has even a positive value at $\rho_{graft} > 0.2$, which means there is no attractive interaction anymore and a dispersed state becomes thermodynamically stable. This suggests that the grafting of ATMSs onto CB surface should increase the dispersibility of CB fillers, thereby enhancing the dielectric properties of the composites in experiments.

In Fig. 4(e), we plot ΔF_1 and ΔF_2 as a function of chain length (n_{chain}) of ATMSs. Both ΔF_1 and ΔF_2 increase as the longer chains are grafted. This is because the longer chains are likely to lose more conformational entropy. Moreover, the increase of ΔF_1 and ΔF_2 with respect to n_{chain} is more prominent as the grafting density increases. This indicates that the dispersibility of CB fillers is improved by grafting ATMSs onto the surface. However, when the concentration of residual ATMSs becomes higher, it would decrease the CB dispersibility and make CB fillers re-agglomerate, for which we believe the non-monotonic trend of the dielectric constant as a function of the ATMS content in experiments (Fig. 2). We calculate $F(h)$ for a given set of $(n_{chain}, \rho_{graft}) = (6,\ 0.2)$ but different values of the residual ATMS concentration, $\rho_{residual}$. As shown in Fig. 4(f), the attractive well becomes deeper and the repulsive barrier becomes lower as $\rho_{residual}$ increases from 0 to 0.05. When two CB particles approach each other, it is entropically unfavorable for residual ATMSs to be located between two CB particles due to depletion effect [39]. Fig. 4(g) shows simulation snapshots taken when they are far apart ($h = 10$) and are sufficiently close with chains in contact ($h \approx 1.8$). Because residual ATMSs between two CB particles in proximity have less number of possible conformations than residual ATMSs in PDMS mixture, residual ATMSs are likely to be pushed out from the space between two CB particles, which creates an entropic attraction between CB particles. This is why both ΔF_1 and ΔF_2 decrease with an increase in $\rho_{residual}$, and the dispersibility of CBs deteriorates with residual ATMSs in the mixture. As the dispersibility of CBs deteriorates after a certain amount of ATMS content due to the presence of residual ATMS molecules, the dielectric constant would decrease accordingly as shown in experiments (Fig. 2).

3.4. Application of CB-embedded PDMS composites to capacitive pressure sensors

While previous capacitive pressure sensors based on delicate microstructures such as pyramid-shaped pure PDMS films show the high sensitivity at light input loading, they present relatively slow dynamic response and low reliability at heavy input loadings [21,22]. Whereas, the flat-structured sensor has a reliable response over the entire loading range [40]. However, these flat-structured sensors suffer from low sensitivity, which is attributed to the small distance change between two electrodes and low dielectric constant of the elastomers. In this context, the capacitive pressure sensors based on the flat structure were fabricated, and the ODTMS modied-$CB_{2wt\%}$/PDMS composites were used as a dielectric elastomer to improve the sensor performance despite small distance change (Fig. 5(a)).

To investigate the effect of dielectric constant of the elastomers between two electrodes on the capacitance change, the pressure sensors

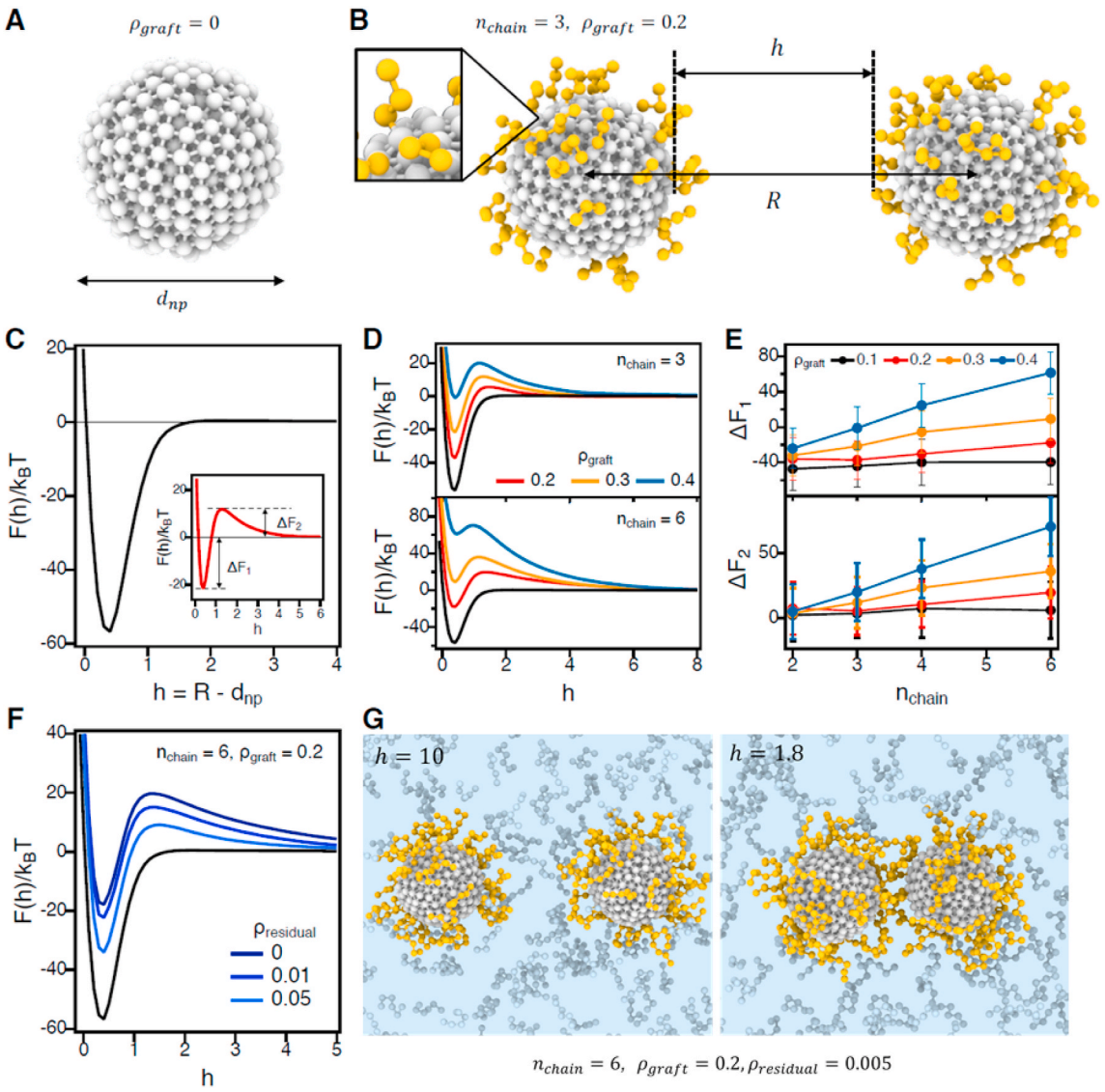

Fig. 4. Simulation results of CB-embedded PDMS dielectric composites. (a) A simulation model for p-CB filler comprised of 500 monomers (white particles). (b) Yellow particles indicate alkyltrimethoxysilane (ATMS) molecules grafted permanently onto the CB surface. SMD simulations are conducted to calculate the free energy along a gap distance, $h = R - d_{np}$. (c) $F(h)$ of two CBs without any ATMS molecules. (Inset) $F(h)$ of two CBs with ATMS molecules of $(n_{chain}, \rho_{graft}, \rho_{residual}) = (3, 0.3, 0)$. (d) $F(h)$ for different ρ_{graft} for (upper) $n_{chain} = 3$ and (lower) $n_{chain} = 6$ with residual ATMS molecules ($\rho_{residual} = 0$). (e) ΔF_1 and ΔF_2 are plotted as a function of n_{chain} with different ρ_{graft}. (f) $F(h)$ for different $\rho_{residual}$ with fixed $n_{chain} = 6$ and $\rho_{graft} = 0.2$. (g) Simulation snapshots when two CBs are far apart (left) and are in contact (right). Grey particles represent residual ATMSs that are not grafted onto CB surface. (For interpretation of the references to colour in this figure legend, the reader is referred to the Web version of this article.)

were prepared using three different dielectric elastomers: (1) pure PDMS ($\varepsilon = 3.4$ at 1 kHz), (2) CB/PDMS-I ($\varepsilon = 59$ at 1 kHz), and (3) CB/PDMS-II ($\varepsilon = 156$ at 1 kHz). The dielectric constant of the composites was controlled by varing the ODTMS content in 2 wt% CB/PDMS mixture (Fig. S8). We evaluated the sensor performance as a function of the input pressure as shown in Fig. S9. Without input pressure, three sensors based on pure PDMS, CB/PDMS-I and CB/PDMS-II show the initial capacitance of 3.08, 52.39 and 139.57 pF at 1 kHz, respectively (Fig. 5(b)). As the input pressure increases to 312 kPa, the capacitance increases to 3.21, 54.08 and 145.58 pF for pure PDMS-, CB/PDMS-I-, and CB/PDMS-II-based sensors, respectively. Under loading conditions, the capacitance change is dramatically improved with an increase of the dielectric constant. While the pure PDMS-based sensor shows about 0.13 pF capacitance change, the CB/PDMS-I- and CB/PDMS-II-based sensors exhibit 1.69 and 6.01 pF capacitance changes, respectively, which are approximately 13 and 46-fold larger than that of the pure PDMS-based sensor (Fig. 5(c)). The hysteresis errors with respect to the maximum output are 8.33, 6.31 and 8.39% for pure PDMS-, CB/PDMS-I-, and CB/PDMS-II-based sensors, respectively, thus indicating that the hysteresis errors have the same values regardless of the dielectric constant. Additionally, the capacitance changes of the three sensors were characterized as a function of the frequency (Fig. S10). While the pure PDMS-based sensor shows little change in the capacitance change, the capacitance changes of the composite-based sensors decrease as the frequency increases from 1 to 50 kHz. It is attributed to the fact that the dielectric constant of the composites decreases with increasing the frequency as shown in Fig. S8. Fig. 5(d) shows the capacitance ratio of the composite-based sensor to the pure PDMS-based one as a function of the input pressure. The capacitance ratios of CB/PDMS-I and II to the pure PDMS-based sensor are 17 and 45, respectively, and these values are constant regardless of the input pressure. These results are entirely consistent with the permittivity ratios of two composites to the pure PDMS, demonstrating that the permittivity of dielectric layer plays a critical role in the sensor sensitivity.

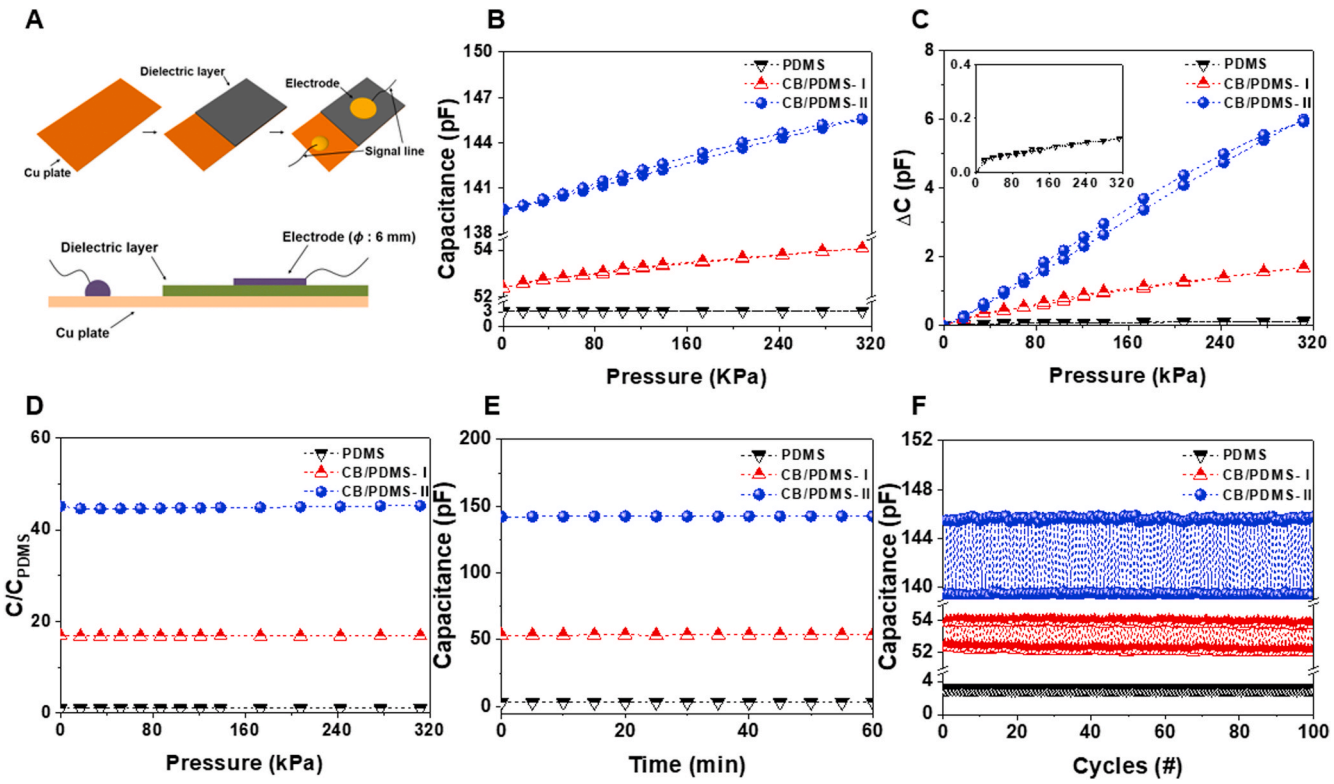

Fig. 5. Performance of three pressure sensors. (a) Schematic illustration showing the preparation of pressure sensor and its dimension. (b) Capacitance, (c) capacitance change, and (d) capacitance ratio of the composite-based sensor to the pure PDMS-based one as a function of the input pressure. (e) Drift characteristics of three sensors at the constant pressure (312 kPa) for 60 min. (f) Capacitances of three sensors under loading (312 kPa) and unloading conditions as a function of the number of loading cycles.

The drift characteristics of each sensor was examined at the constant pressure (312 kPa) for 60 min (Fig. 5(e)). The drift errors are 0.3, 0.5 and 0.3% for pure PDMS-, CB/PDMS-I-, and CB/PDMS-II-based sensors, respectively, indicating an excellent stability. Fig. 5(f) presents the cycling tests showing the capacitances of three sensors under loading (312 kPa) and unloading conditions versus the number of loading cycles. Three sensors exhibit a constant load response during 100 cycles. The capacitance change is constant, and the deviation from the average value is less than 0.4% for three sensors. These results demonstrate that the flat-structured pressure sensor shows the reliable response over the entire loading range. More importantly, the CB/PDMS based pressure sensor has an enhanced tolerance to external noise sources, due to the large capacitance change derived from high dielectric constant.

4. Conclusion

We have demonstrated a new concept of ODTMS-modified $CB_{3wt\%}$/PDMS composites exhibiting an enhanced dielectric constant of 1090 with low loss tangent as low as 0.45 at 100 Hz *via* a one-pot process. This dielectric constant is 145-fold higher than that of the p-$CB_{3wt\%}$/PDMS composites without ODTMS, currently one of the highest dielectric constants with low loss tangent reported for dielectric elastomers. These results are attributed to the CB particles well-dispersed in PDMS without loss of their intrinsic electrical properties. Experimental and simulation studies show that the dielectric properties of CB/PDMS composites strongly depend on the CB dispersion in the PDMS matrix, which is affected by the chain length of ATMS used as a dispersant and the amount of residual ATMSs. As a proof of concept, the flat-structured capacitive pressure sensor based on CB/PDMS composites has been demonstrated. The sensor based on CB/PDMS composites with high dielectric constant of 156 at 1 kHz shows approximately 46-fold larger capacitance change than the pure PDMS based sensor, thus indicating that the sensor sensitivity can be significantly improved without additional micro-structuring. Furthermore, this pressure sensor exhibits large capacitance changes despite small distance changes between two electrodes, thus enhancing a tolerance to external noise sources. The drift characteristics and cycling tests present the excellent reliability at heavy input loadings. The strategy proposed in this study shows great potential for capacitive pressure sensors, which should respond to various input pressures.

CRediT authorship contribution statement

Youngpyo Ko: Methodology, Investigation, Visualization, Writing - original draft. **Hyungsuk Yoon:** Methodology, Investigation, Visualization, Writing - original draft. **Seulki Kwon:** Software, Formal analysis, Writing - original draft. **Hyunjung Lee:** Resources. **Min Park:** Resources. **Insu Jeon:** Resources. **Jung Ah Lim:** Methodology, Investigation. **Seungjun Chung:** Methodology, Investigation. **Sang-Soo Lee:** Conceptualization, Resources, Supervision. **Bong June Sung:** Conceptualization, Resources, Supervision. **Jong-Ho Kim:** Conceptualization, Resources, Supervision. **Heesuk Kim:** Conceptualization, Resources, Supervision, Writing - review & editing.

Declaration of competing interest

The authors declare that they have no known competing financial interests or personal relationships that could have appeared to influence the work reported in this paper.

Acknowledgements

This research was supported by the National Research Foundation of Korea (NRF-2019R1A2C2091094).

Appendix A. Supplementary data

Supplementary data to this article can be found online at https://doi.org/10.1016/j.compositesb.2020.108337.

References

[1] Carpi F, Bauer S, Rossi DD. Stretching dielectric elastomer performance. Science 2010;330:1759–61.
[2] Tu NDK, Noh Y-S, Ko Y, Kim J-H, Kang CY, Kim H. Enhanced electromechanical performance of P(VDF-TrFE-CTFE) thin films hybridized with highly dispersed carbon blacks. Compos B Eng 2018;152:133–8.
[3] Chen Y, Zhao H, Mao J, Chirarattananon P, Helbling EF, Hyun N-SP, Clarke DR, Wood RJ. Controlled flight of a microrobot powered by soft artificial muscles. Nature 2019;575:324–9.
[4] Ke K, McMaster M, Christopherson W, Singer KD, Manas-Zloczower I. Effects of branched carbon nanotubes and graphene nanoplatelets on dielectric properties of thermoplastic polyurethane at different temperatures. Compos B Eng 2019;166:673–80.
[5] Shanker R, Cho S, Choe A, Kim MP, Khan Z, Kang S, Ko H. Solution-processable, high-performance flexible electroluminescent devices based on high-k nanodielectrics. Adv Funct Mater 2019;29:1904377.
[6] Bartlett MD, Fassler A, Kazem N, Markvicka EJ, Mandal P, Majidi C. Stretchable, high- k dielectric elastomers through liquid-metal Inclusions. Adv Mater 2016;28:3726–31.
[7] Zeraati AS, Arjmand M, Sundararaj U. Silver nanowire/MnO_2 nanowire hybrid polymer nanocomposites: materials with high dielectric permittivity and low dielectric loss. ACS Appl Mater Interfaces 2017;79:14328–36.
[8] Fan B, He D, Liu Y, Zhou M, Zhang C, Bai J. Improved dielectric properties achieved by blending PP and PVDF. IET Nanodielectr 2019;2:78–81.
[9] Chen Y, Kong Z, Chen W, Xiao L, Yuan Y, Li Z, Zhuang Q. In situ synthesis of high dielectric constant GNPs/PBO nanocomposites with enhanced thermostability. IET Nanodielectr 2019;2:97–102.
[10] Yang D, Tian M, Li D, Wang W, Ge F, Zhang L, Zhang. Enhanced dielectric properties and actuated strain of elastomer composites with dopamine-induced surface functionalization. J Mater Chem A 2013;1:12276–84.
[11] Dang Z-M, Yuan J-K, Yao S-H, Liao R-J. Flexible nanodielectric materials with high permittivity for power energy storage. Adv Mater 2013;25:6334–65.
[12] Prateek, Thakur VK, Gupta RK. Recent progress on ferroelectric polymer-based nanocomposites for high energy density capacitors: synthesis, dielectric properties, and future aspects. Chem Rev 2016;116:4260–317.
[13] Sun H, Zhang H, Liu S, Ning N, Zhang L, Tian M, Wang Y. Interfacial polarization and dielectric properties of aligned carbon nanotubes/polymer composites: the role of molecular polarity. Compos Sci Technol 2018;154:145–53.
[14] Jang H, Yoon H, Ko Y, Choi J, Lee S-S, Jeon I, Kim J-H, Kim H. Enhanced performance in capacitive force sensors using carbon nanotube/polydimethylsiloxane nanocomposites with high dielectric properties. Nanoscale 2016;8:5667–75.
[15] Fan B, Liu Y, He D, Bai J. Achieving polydimethylsiloxane/carbon nanotube (PDMS/CNT) composites with extremely low dielectric loss and adjustable dielectric constant by sandwich structure. Appl Phys Lett 2018;112:052902.
[16] Huang M, Tunnicliffe LB, Zhuang J, Ren W, Yan H, Busfield JJC. Strain-dependent dielectric behavior of carbon black reinforced natural Rubber. Macromolecules 2016;49:2339–47.
[17] Babu I, With GD. Enhanced electromechanical properties of piezoelectric thin flexible films. Compos Sci Technol 2014;104:74–80.
[18] Zhao H, Xia Y-J, Dang Z-M, Zha J-W, Hu G-H. Composition dependence of dielectric properties, elastic modulus, and electroactivity in (carbon black-$BaTiO_3$)/silicone rubber nanocomposites. J Appl Polym Sci 2013;127:4440–5.
[19] Wongtimnoi K, Guiffard B, Moortèle AB-VD, Seveyrat L, Cavaillé J-Y. Electrostrictive thermoplastic polyurethane-based nanocomposites filled with carboxyl-functionalized multi-walled carbon nanotubes (MWCNT-COOH): properties and improvement of electromechanical activity. Compos Sci Technol 2013;85:23–8.
[20] Galantini F, Bianchi S, Castelvetro V, Gallone G. Functionalized carbon nanotubes as a filler for dielectric elastomer composites with improved actuation performance. Smart Mater Struct 2013;22:055025.
[21] Kang S, Lee J, Lee S, Kim S, Kim J-K, Algadi H, Al-sayari S, Kim D-E, Lee T. Highly sensitive pressure sensor based on bioinspired porous structure for real-time tactile sensing. Adv. Electron. Mater. 2016;2:1600356.
[22] Mannsfeld SCB, Tee BC-K, Stoltenberg RM, Chen CVH-H, Barman S, Muir BVO, Sokolov AN, Reese C, Bao Z. Highly sensitive flexible pressure sensors with microstructured rubber dielectric layers. Nat Mater 2010;9:859–64.
[23] Zhang H, Wei X, Ding Y, Jiang Z, Ren J. A low noise capacitive MEMS accelerometer with anti-springstructure. Sens. Actuator A Phys. 2019;296:79–86.
[24] Hu Y, Huang L, Rieutort-Louis W, Sanz-Robinson J, Wagner S, Sturm JC, Verma N. ISSCC, 3D Gesture-sensing system for interactive displays based on extended-range capacitive sensing. 2014. San Francisco, CA, USA, Feb.
[25] Plimpton S. Fast parallel algorithms for short-range molecular dynamics. J Comput Phys 1995;177:1–19.
[26] Jarzynski C. Nonequilibrium equality for free energy differences. Phys Rev Lett 1997;78:2690–3.
[27] Park S, Khalili-Araghi F. Free energy calculation from steered molecular dynamics simulations using Jarzynski's equality. J Chem Phys 2003;119:3559–66.
[28] Lee JN, Park C, Whitesides GM. Solvent compatibility of poly(dimethylsiloxane)-based microfluidic devices. Anal Chem 2003;75:6544–54.
[29] Akcora1 P, Liu H, Kumar SK, Moll J, Li Y, Benicewicz BC, Schadler LS, Acehan D, Panagiotopoulos AZ, Pryamitsyn V, Ganesan V, Ilavsky J, Thiyagarajan P, Colby RH, Douglas JF. Anisotropic self-assembly of spherical polymer-grafted nanoparticles. Nat Mater 2009;8:354–9.
[30] Zhang S-P, Song H-O. Supramolecular graphene oxide-alkylamine hybrid materials: variation of dispersibility and improvement of thermal stability. New J Chem 2012;36:1733–8.
[31] Wood W, Kumar S, Zhong W-H. Synthesis of organosilane-modified carbon nanofibers and influence of silane coating thickness on the performance of polyethylene nanocomposites. Macromol Mater Eng 2010;295:1125–35.
[32] Byun S-H, Sim JY, Zhou Z, Lee J, Qazi1 R, Walicki MC, Parker KE, Haney MP, Choi SH, Shon A, Gereau GB, Bilbily J, Li S, Liu Y, Yeo W-H, McCall JG, Xiao J, Jeong J-W. Mechanically transformative electronics, sensors, and implantable devices. Sci. Adv. 2019;5:eaay0418.
[33] Yoon JI, Choi KS, Chang SP. A novel means of fabricating microporous structures for the dielectric layers of capacitive pressure sensor. Microelectron Eng 2017;179:60–6.
[34] Wan Y, Qiu Z, Hong Y, Wang Y, Zhang J, Liu Q, Wu Z, Guo CF. A highly sensitive flexible capacitive tactile sensor with sparse and high-aspect-ratio microstructures. Adv. Electron. Mater. 2018;4:1700586.
[35] Park SW, Das PS, Park JY. Development of wearable and flexible insole type capacitive pressure sensor for continuous gait signal analysis. Org Electron 2018;53:213–20.
[36] Liu S, Sun H, Ning N, Zhang L, Tian M, Zhu W, Chan TW. Aligned carbon nanotubes stabilized liquid phase exfoliated graphene hybrid and their polyurethane dielectric elastomers. Compos Sci Technol 2016;125:30–7.
[37] Barick AK, Tripathy DK. Preparation, characterization and properties of acid functionalized multi-walled carbon nanotube reinforced thermoplastic polyurethane nanocomposites. Mater Sci Eng B 2011;176:1435–47.
[38] Kea K, McMasterb M, Christophersonb W, Singerb KD, Manas-Zloczower I. Effects of branched carbon nanotubes and graphene nanoplatelets on dielectric properties of thermoplastic polyurethane at different temperatures. Compos B Eng 2019;166:673–80.
[39] Mao Y, Cates ME, Lekkerkerker HNW. Depletion force in colloidal systems. Physica A 1995;222:10–24.
[40] Lipomi DJ, Vosgueritchian M, Tee BC-K, Hellstrom SL, Lee JA, Fox CH, Bao Z. Skin-like pressure and strain sensors based on transparent elastic films of carbon nanotubes. Nat Nanotechnol 2011;6:788–92.